Solid solubility and transport properties of Ce1-xNdx02-δ nanocrystalline solid solutions by a sol-gel route

doi: 10.1557/JMR.2001.0442

Solid solubility and transport properties of $Ce_{1-x}Nd_xO_{2-\delta}$ nanocrystalline solid solutions by a sol-gel route

Liping Li[a] and Xiaomin Lin
Physics Department, Jilin University, Changchun 130023, People's Republic of China
Guangshe Li[b] and Hiroshi Inomata
Research Center of Supercritical Fluid Technology, Department of Chemical Engineering, Tohoku University, Sendai 980-8579, Japan

(Received 20 February 2001; accepted 27 August 2001)

$Ce_{1-x}Nd_xO_{2-\delta}$ ($x = 0.05$ to 0.55) nanocrystalline solid solutions were prepared by a sol-gel route. X-ray diffraction analysis showed that $Ce_{1-x}Nd_xO_{2-\delta}$ crystallized in a cubic fluorite structure. The lattice parameter for the solid solutions increased linearly with the dopant content. The solid solubility of Nd^{3+} in ceria lattice was determined to be about $x = 0.40$ in terms of the nearly constant lattice parameters at a dopant level larger than $x = 0.40$. First-order Raman spectra for $Ce_{1-x}Nd_xO_{2-\delta}$ at a lower dopant content exhibited one band associated with the F_{2g} mode. At higher dopant contents, F_{2g} mode became broadened and asymmetric, and a new broad band appeared at the higher frequency side of the F_{2g} mode. This new band was assigned to the oxygen vacancies. The electron paramagnetic resonance spectrum for $x = 0.05$ showed the presence of O_2^- adsorbed on sample surface at $g = 2.02$ and 2.00 and of Ce^{3+} with a lower symmetry at $g = 1.97$ and 1.94. Further increasing dopant content led to the disappearance of the signals for O_2^-. Impedance spectra showed the bulk and grain boundary conduction in the solid solutions. The bulk conduction exhibited a conductivity maximum and an activation energy minimum with increasing dopant content. $Ce_{0.80}Nd_{0.20}O_{2-\delta}$ was determined to give promising conduction properties such as a relatively high conductivity of $\sigma_{700\,^\circ C} = 2.44 \times 10^{-2}$ S cm^{-1} and moderate activation energy of $E_a = 0.802$ eV. The variations of conductivity and activation energy were explained in terms of relative content of oxygen vacancies $V_{\ddot{O}}$ and defect associations $\{Ce_{Ce}'V_{\ddot{O}}\}/\{Nd_{Ce}'V_{\ddot{O}}\}$.

I. INTRODUCTION

Solid electrolytes are crucial components for electrochemical devices such as solid oxide fuel cell and oxygen separation membranes.[1] Enhanced ionic conductivity and highly thermal stability are two important parameters for the applications of electrolytes. The electrolytes widely investigated are fluorite-type oxides such as yttrium-stabilized zirconia (YSZ);[2] however doped ceria has been shown to be an alternative electrolyte due to its much higher oxide-ion conductivity than YSZ and relatively high thermal stability.[3–6] It is well known that oxide-ion hopping in the doped ceria is determined by the intrinsic and extrinsic oxygen vacancies. Intrinsic oxygen vacancies can be produced via the reduction equilibrium of Ce^{3+}/Ce^{4+} in the doped ceria, which might account for the electronic component in the total conduction, while the extrinsic oxygen vacancies are controlled by the substitution of aliovalent ions for Ce^{4+} in the lattice.

In general, the doped fluorite solid solutions with a larger lattice parameter allow a higher ionic conductivity. As a consequence, strong correlation can be expected between the ionic conduction and dopant size in the fluorite lattice.[7] Aliovalent dopants in ceria could produce lattice distortions due to the differences in charge and ionic size from Ce^{4+}. It is reasonable that the lattice distortions have some pronounced influences on the relative content of Ce^{3+}, ionic conductivity, and thermal stability. Recently, we studied in detail the preparation and transport properties of $Ce_{1-x}M^{3+}{}_xO_{2-\delta}$ (M = Bi, Eu, Tb) and found that (i) relative content of Ce^{3+} in $Ce_{1-x}Bi^{3+}{}_xO_{2-\delta}$ solid solutions decreased with the increment of dopant Bi^{3+}, and these solid solutions have a relatively high thermal stability. (ii) $Ce_{1-x}Eu^{3+}{}_xO_{2-\delta}$ solid solutions are thermally stable, while $Ce_{1-x}Tb^{3+}{}_xO_{2-\delta}$

[a]Present address: Department of Materials Science, Caltech, Pasadena, California 91125.
[b]Address all correspondence to this author.
e-mail: guangshe@hotmail.com

solid solutions are metastable phases, which would be destabilized at high temperatures into fluorite phases accompanied by a partial oxidation from Tb^{3+} to Tb^{4+}, even though both solid solutions contain some amounts of Ce^{3+}.[8,9] In combination with the thermal stability and relative ionic size of these trivalent dopants to Ce^{4+} (i.e., 0.117 nm for Bi^{3+}, 0.1066 nm for Eu^{3+}, 0.104 nm for Tb^{3+}, and 0.097 nm for Ce^{4+} in 8-fold),[10] it is interesting to find that the doped ceria with a larger dopant probably has a relatively high thermal stability. To further confirm such a trend, we selected the dopant Nd^{3+} with an intermediate ionic size (0.1109 nm) between those of Bi^{3+} and Eu^{3+} with an aim of obtaining a series of ceria-based solid solutions showing both enhanced ionic conductivity and high thermal stability.

$Ce_{1-x}Nd_xO_{2-\delta}$ solid solutions by solid-state reactions usually exhibit some second phases even at a dopant level of 10 mol%, which is lower than the solid solubility of the rare-earth ions in ceria lattice.[7] In this paper, we prepared single-phase $Ce_{1-x}Nd_xO_{2-\delta}$ nanocrystalline solid solutions over a wide composition range by a sol-gel route. The solid solubility, ionic conductivity, and thermal stability for these solid solutions were determined and discussed.

II. EXPERIMENTAL PROCEDURE

$Ce_{1-x}Nd_xO_{2-\delta}$ nanocrystalline solid solutions were prepared by a sol-gel route using analytic reagent grade chemicals $Ce(NO_3)_3 \cdot 6H_2O$ and Nd_2O_3 as the starting materials. The mixture of $Ce(NO_3)_3 \cdot 6H_2O$ and Nd_2O_3 with the molar ratios of $Ce_{1-x}Nd_xO_{2-\delta}$ ($x = 0.05, 0.10, 0.20, 0.30, 0.35, 0.40, 0.50, 0.55$) was first dissolved into 1 M nitrate solution. A given concentrated citric acid was added dropwise into the mixture during stirring. The molar ratio of Nd to citric acid was fixed as 1.0:1.2. The wet gel was formed after the solution was mixed by magnetic stirring at 80 °C for 6 h. A dried gel was obtained after the wet gel was baked at 150 °C for 2 h. The dried gel was heated at 800 °C in air for 10 h. The powdered samples were pressed into pellets with a dimension of Φ 13×1 mm^2, and then the pellet samples were sintered at 1100 °C for 10 h. All pellets were found to have densities higher than 93% of theoretical values.

The structures for the solid solutions were identified by means of powder x-ray diffraction (XRD) on a Rigaku, D/max-γA 12kW XRD diffractometer (Tokyo, Japan) with Cu K_α radiation at room temperature. The lattice parameters were calculated by least-squares methods using the diffraction peaks below 80°. The average grain sizes (D) were calculated from the XRD peak (111) using the Scherrer formula.

Raman spectra of the solid solutions were obtained with a J-YT64000 spectrometer (Jobin Yvon Ltd., Hampshire, UK) with an Ar^+-ion laser at an excitation of 488 nm. The resolution was 1 cm^{-1}. Energy dispersive x-ray analysis (EDX) for the pellet samples obtained after heating at 800 °C was examined by electronic microscopy (H-8100IV transition electronic microscopy) (Hitachi Ltd., Tokyo, Japan) under an accelerated voltage of 200 kV. The quantitative analysis results confirmed that the molar ratios of Nd to Ce in the solid solutions were very near to the initial ones.

Electron paramagnetic resonance (EPR) measurements were performed on a Bruker ER200D spectrometer. A frequency of approximately 9.61 GHz was used for a dual-purpose cavity operation. The magnetic field of 0.32 mT was modulated at 100 KHz. A microwave power of about 2.05 mW was employed. Reference signals of Mn^{2+} ions in MgO crystals were used as the standard for the precise effective *g*-factor value.

The opposite sides of the pellet samples were coated with silver paste and heated at 550 °C in air for half an hour so the organic components in the paste could be completely removed. The ionic conductivity for the pellet samples was measured using Solarton 1260 impedance/gain-phase analyzer (Hampshire, UK) with the alternating current having a frequency between 5 Hz and 13 MHz at an amplitude of 50 mV in the temperature range of 350–750 °C in air.

III. RESULTS AND DISCUSSION

XRD patterns for $Ce_{1-x}Nd_xO_{2-\delta}$ samples obtained when the dried gels were heated at 800 °C are shown in Fig. 1, while XRD data for Nd_6O_{11} (JCPDS No. 45-87) are illustrated for comparison. All diffraction peaks for $Ce_{1-x}Nd_xO_{2-\delta}$ at $x < 0.4$ were highly symmetric and matched well with the diffraction data for the standard fluorite structure. The average grain sizes of all samples were within a range of 23–32 nm, as they were calculated from the main peak (111) by using the Scherrer formula. No XRD peak was observed for the impurity phases, such as the component oxides Nd_2O_3 and CeO_2, by scaling up the XRD patterns in Fig. 1. This result is clearly different from that by solid-state reactions. In the latter case, some second phases were readily formed even at a relatively low dopant content. Therefore, the XRD data in Fig. 1 for the present solid solutions could be indexed in a cubic symmetry. With increasing dopant content, the diffraction peaks systematically shifted toward lower angles, as clearly seen in Fig. 2 by the enlargement of the peaks (220) of Fig. 1, which indicated the formation of $Ce_{1-x}Nd_xO_{2-\delta}$ nanocrystalline solid solutions. Figure 3 shows the relationship between the lattice parameter and dopant content. It can be seen that all lattice parameters for $Ce_{1-x}Nd_xO_{2-\delta}$ solid solutions were larger than the value of 0.5411 nm for pure ceria (JCPDS No. 34-394), and that the lattice parameter increased linearly with the increment of dopant content. At dopant

contents higher than $x = 0.40$, the lattice parameter remained nearly the constant, which indicated that the solid solubility of Nd^{3+} in ceria is probably $x = 0.40$. The broadening effect from the nanocrystalline solid solutions probably obscure the diffraction peaks from the second phase of Nd_6O_{11} due to its strongest peak being very close to the main peak (111) of the solid solution at $x = 0.40$ (see Fig. 1).

For an understanding of the linear relationship in Fig. 3, one should take into account the effects from the oxygen vacancy $V_{\ddot{O}}$, relative content of Ce^{3+}, and substitution of Nd^{3+} at Ce^{4+} sites in the solid solutions. In $Ce_{1-x}Nd_xO_{2-\delta}$, every two Nd^{3+} or Ce^{3+} arising from the reduction equilibrium of Ce^{3+}/Ce^{4+} would generate one oxygen vacancy $V_{\ddot{O}}$[8], while localized defect associations $\{Ce_{Ce}'V_{\ddot{O}}\}/\{Nd_{Ce}'V_{\ddot{O}}\}$ appeared at the higher dopant contents. The oxygen vacancies $V_{\ddot{O}}$ are expected to exhibit some lattice constraint;[11] this is the opposite of what results from the cation substitution of Nd^{3+} for Ce^{4+}. It should be noted that in the doped fluorite lattice, there exist some changes of the relative contents of the oxygen vacancy $V_{\ddot{O}}$ and the localized defect associations[8,9] (i.e., $\{Ce_{Ce}\ 'V_{\ddot{O}}\}$ and $\{Nd_{Ce}\ 'V_{\ddot{O}}\}$ for the present $Ce_{1-x}Nd_xO_{2-\delta}$) with increasing dopant contents; e.g., the number of oxygen vacancies $V_{\ddot{O}}$ in the solid solutions would first increase with the dopant content and reach a maximum at a certain dopant content, and then the defect associations begin to form.[4] When the dopant content was increased up to $x = 0.40$, the linear increase of lattice parameter was mainly determined by the increase of effective ionic size and by the small lattice constraint from oxygen vacancies. Further increasing dopant content above $x = 0.40$ probably led to a constant content of

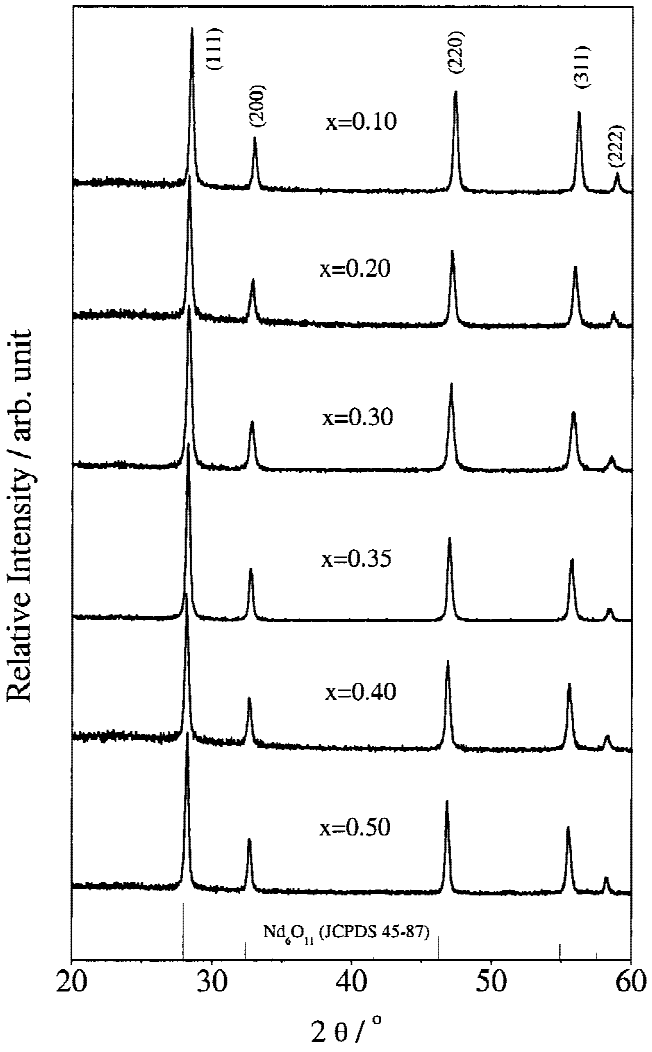

FIG. 1. XRD patterns for $Ce_{1-x}Nd_xO_{2-\delta}$ nanocrystalline solid solutions obtained by heating the dried gels at 800 °C for 10 h.

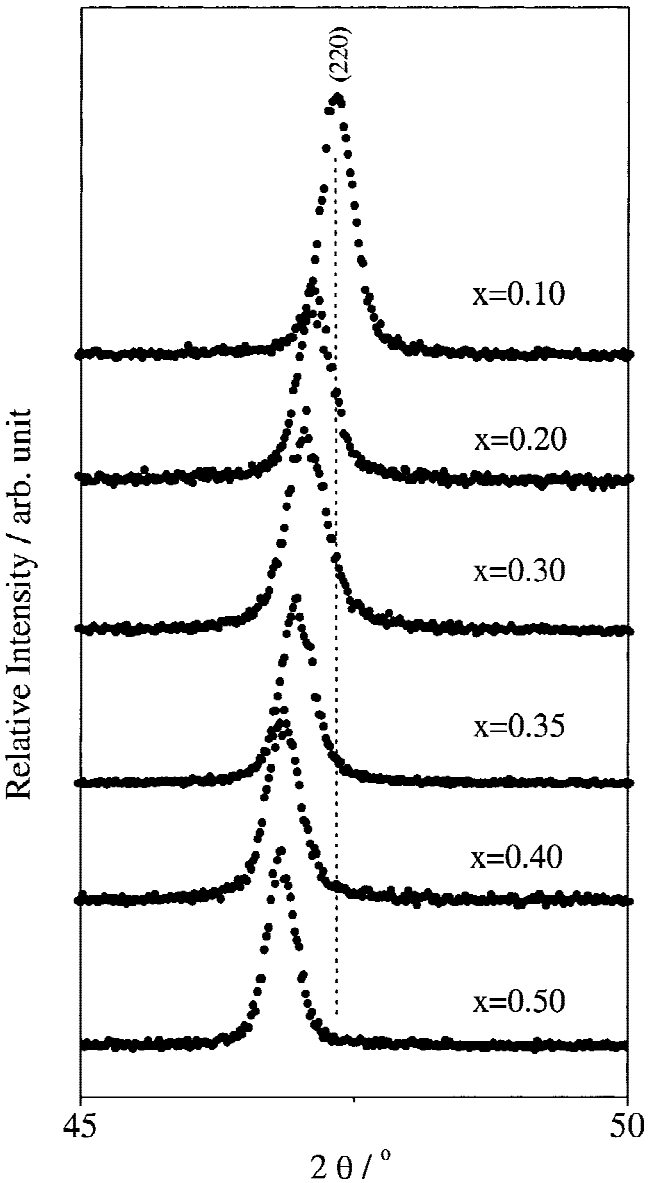

FIG. 2. Enlargement of the diffraction line (220) of Fig. 1.

Nd^{3+} in ceria lattice, while the excess Nd^{3+} was separated in the form of Nd_6O_{11} as described above. The oxygen vacancies and defect associations are determined by the following Raman and impedance spectra.

Typical Raman spectra for $Ce_{1-x}Nd_xO_{2-\delta}$ nanocrystalline solid solutions are shown in Fig. 4. It can be seen that only one predominant band was observed at 448 cm^{-1} with a dopant content lower than $x = 0.10$, which is assigned to the F_{2g} mode. In fact, for the cubic fluorite structure with a space group of *Fm*3*m*, group theory predicts one triply degenerate Raman active optical phonon of Γ_{25} symmetry (F_{2g}) and two infrared active phonons of Γ_{15} symmetry (F_{1u}).[12] Therefore, the first-order Raman spectra for $Ce_{1-x}Nd_xO_{2-\delta}$ should consist of only one Raman band of F_{2g} mode. However, as shown in Fig. 4, with increasing dopant content above $x = 0.10$, the F_{2g} mode broadened and became asymmetric, while a new broad peak appeared at above 550 cm^{-1}. This new peak can be assigned to the oxygen vacancies in the fluorite lattice.[13] Further increasing dopant content did not lead to any obvious shift of F_{2g} mode. It is well known that the F_{2g} mode can be viewed as a symmetric breathing mode of the oxygen atoms around the framework cerium ions. The mode frequency should be nearly independent of the cation mass[14] because the lattice expansion due to larger cation substitution would cause a red shift of the F_{2g} mode and a blue shift of the oxygen vacancy mode.[13] For $x = 0.05$, the phonon mode of oxygen vacancies was very weak and could barely be observed due to the extremely low concentration of oxygen vacancies. The phonon mode began to appear at $x = 0.10$, which could be the result of doping effects from Nd^{3+} as well as the intrinsic reduction equilibrium of Ce^{3+}/Ce^{4+}. The content of oxygen vacancies increased with the dopant content, which was confirmed by the increased relative intensity of the oxygen vacancy band to the F_{2g} band shown in Fig. 4.

Our previous studies have shown that EPR technique is efficient in identifying Ce^{3+} in the bulk of ceria-based solid solutions.[8,9] EPR spectra for $Ce_{1-x}Nd_xO_{2-\delta}$ solid solutions recorded at room temperature are shown in Fig. 5. At a dopant level of $x = 0.05$, the EPR spectrum showed four signals with $g = 2.02$, 2.00, 1.97, and 1.94, respectively. According to the literature,[15] the signal with $g = 2.02$ and 2.00 can be assigned to the O_2^- adsorbed on the sample surface, which probably followed such a path:

$$O_2\ (g) + e' = O_2^-\ (ads) \quad .$$

The adsorption is considered to be reversible. The formation of O_2^- could lead to a reduction in the concentration of conduction electrons and hence a lowering

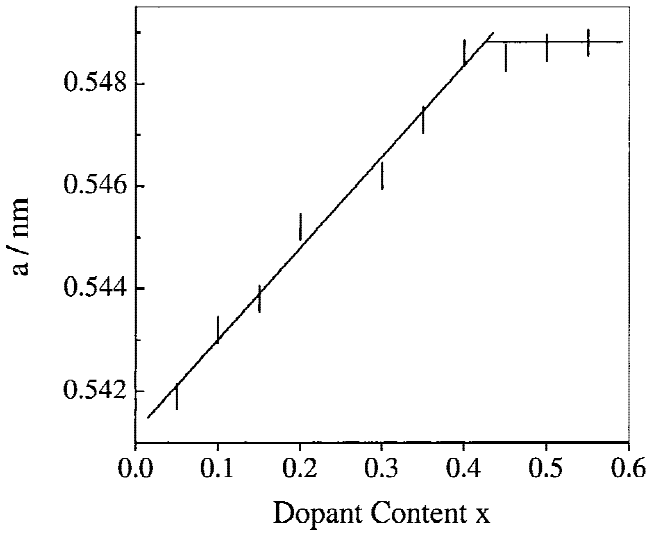

FIG. 3. Lattice parameters for $Ce_{1-x}Nd_xO_{2-\delta}$ nanocrystalline solid solutions as a function of dopant content.

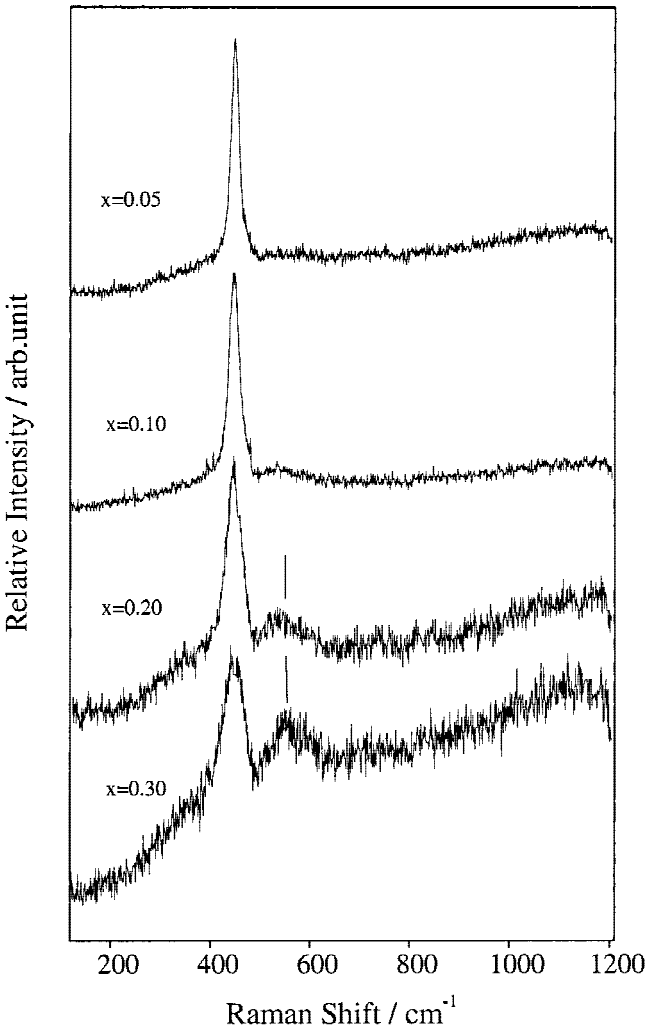

FIG. 4. Raman spectra for $Ce_{1-x}Nd_xO_{2-\delta}$ nanocrystalline solid solutions at room temperature.

electronic component in the total conductivity of the solid solutions, which would be confirmed by following impedance spectra. The assignment of the signal at about $g = 1.97$ remained in controversy; some authors assigned this signal to the quasi-free electrons while others assigned it to Ce^{3+}.[16] In fact, Ce^{3+} located in the lattice site with an axial symmetry is characterized by the EPR signal with $g_{\perp} = 1.96$ and $g_{//} = 1.94$.[8] We also find that Ce^{3+} in an asymmetric field gives a broad EPR signal with a g value of about 2.0.[9] For the present nanocrystalline solid solutions, the lattice distortions could be increased with dopant content due to the oxygen vacancies and larger Nd^{3+}, as reflected by the lattice expansion in Fig. 3. Therefore, a single broad signal could be expected for the present solid solutions at higher dopant contents. In combination with others' work,[15] we assigned the signal with $g = 1.97$ and 1.94 to Ce^{3+} with a low symmetry.

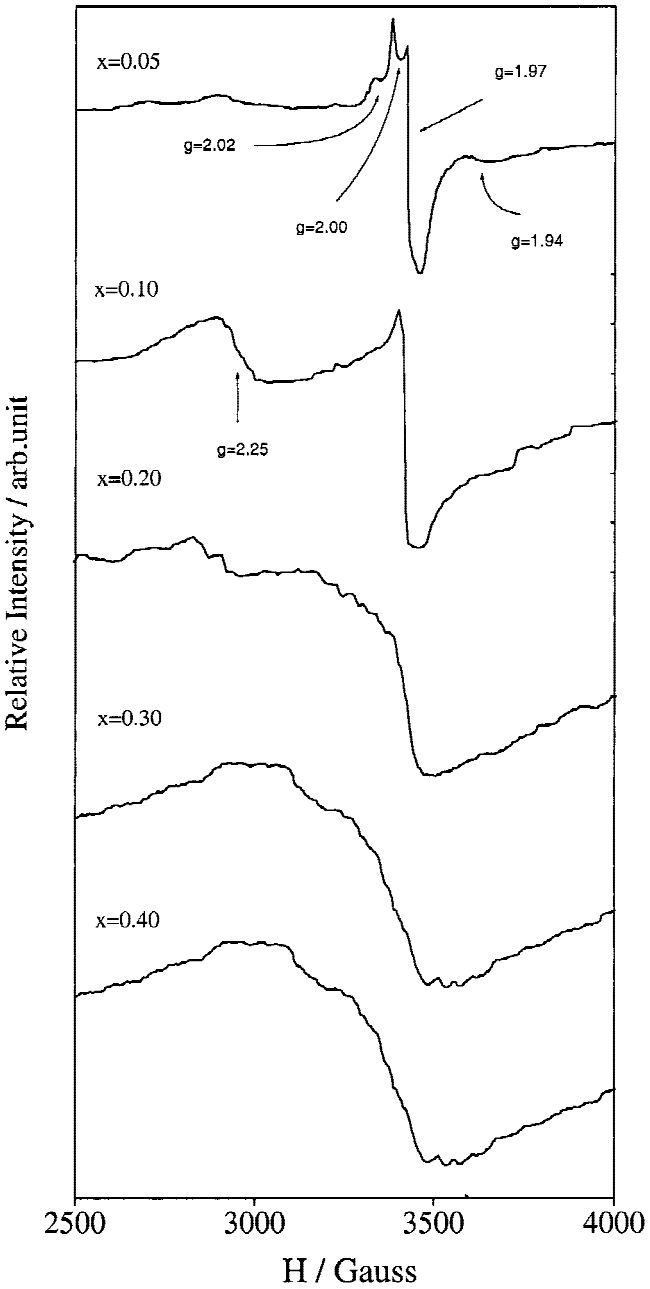

FIG. 5. EPR spectra for $Ce_{1-x}Nd_xO_{2-\delta}$ solid solutions recorded at room temperature.

When the dopant content was increased to $x = 0.10$, as shown in Fig. 5, the signals for Ce^{3+} at $g = 1.94$ and those for O_2^- at $g = 2.02$ and 2.00 were absent, while a new signal with a higher g-factor of 2.25 appeared. The signal observed at $g = 1.97$ indicated that the solid solution contained some amount of Ce^{3+}. Further increase in dopant content led to weakening of the new signal at $g = 2.25$ and of the Ce^{3+} signal at $g = 1.97$. As discussion above, the substitution of Nd^{3+} for Ce^{4+} introduces oxygen vacancies to maintain the charge equilibrium. In such a defective fluorite lattice, Nd^{3+} could be more stable than Ce^{3+}, while most oxygen vacancies would probably be localized around Nd^{3+} by forming defect associations $\{Nd_{Ce}'V_{\ddot{O}}\}$, which would lead to an increase in the coordination number of Ce^{3+} in an axial symmetry. As the content of Nd^{3+} was larger than $x = 0.10$, great amount of oxygen vacancies were introduced in the solid solutions, which could destroy the axial symmetry of electronic field around Ce^{3+}. The signal with $g = 2.25$ for $x = 0.10$ could be associated with the Ce^{3+} in a distortion polyhedron of defect associations $\{Ce_{Ce}'V_{\ddot{O}}\}$. When the dopant content was larger than $x = 0.30$, the signal with $g = 2.25$ became very weak, which was probably due to the reduction of relative content for defect associations $\{Ce_{Ce}'V_{\ddot{O}}\}$. Accordingly, the signal for O_2^- disappeared. On the other hand, the EPR signal centered at $g = 1.97$ shifted to about $g = 2.00$ and broadened, which indicated the strong interactions among the defect associations $\{Ce_{Ce}'V_{\ddot{O}}\}$ and $\{Nd_{Ce}'V_{\ddot{O}}\}$. Similarly, EI-Mallawany *et al.*[17] found a broad signal of $g \sim 2.00$ in the EPR spectrum of $(TeO_2)_{0.95}(CeO_2)_{0.05}$ and ascribed this signal to Ce^{3+}. The present results also showed the reduction equilibrium of Ce^{3+}/Ce^{4+} existing in the solid solutions even at higher dopant levels.

The ionic conductivities for $Ce_{1-x}Nd_xO_{2-\delta}$ solid solutions were determined by alternating current impedance technique on the sintered pellet samples. A typical impedance spectrum for $Ce_{0.80}Nd_{0.20}O_{2-\delta}$ at 500 °C was clearly divided into two semicircles.[18] The small depressed semicircle at the higher frequencies is due to the bulk effect, and the larger semicircle at the low frequencies is ascribed to the grain boundary conduction. It should be noted that no electrode arc was observed, which indicated the absence of the oxygen exchange processes occurred in the interface between electrodes and samples. Such a behavior could be due to the partial

electronic nature of the conductivity in the ceria-based solid solutions arising from the reduction equilibrium of Ce^{3+}/Ce^{3+}.[9]

The intersections of the semicircles with the real part of the impedance (Z′) axis were taken to determine the bulk and gain boundary resistance. Here we emphasized the bulk conduction in $Ce_{1-x}Nd_xO_{2-\delta}$ solid solutions. The temperature dependence of the bulk conductivity for the solid solutions is shown in Fig. 6. It is clear that the conductivity data for these solid solutions gave only one linear region and followed the Arrhenius behavior over the temperature regions studied. These results showed that the conductivity was primarily by oxide ion and the electronic component could be negligible at higher dopant contents consistent with EPR analysis. No break was observed in the conductivity data up to 1000 °C, indicating that $Ce_{1-x}Nd_xO_{2-\delta}$ solid solutions had a relatively high thermal stability. The conductivity at 700 °C and activation energy obtained are given in Table I. The activation energy for ceria in Ref. 19 is also shown for comparison. It can be found that the ionic conductivity

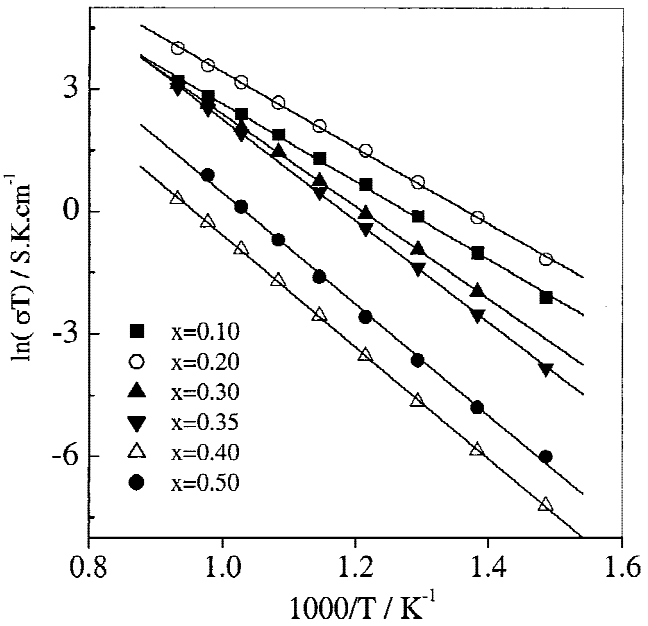

FIG. 6. Temperature dependence of the ionic conductivity for $Ce_{1-x}Nd_xO_{2-\delta}$ solid solutions.

TABLE I. Conductivity data (σ) at 700 °C and activation energy data (E_a) for $Ce_{1-x}Nd_xO_{2-\delta}$ solid solutions.

Dopant content (x)	σ (S cm^{-1})	E_a (eV)
0.00[a]	$<5.0 \times 10^{-3}$	1.96
0.10	1.12×10^{-2}	0.824
0.20	2.44×10^{-2}	0.802
0.30	8.10×10^{-3}	0.976
0.35	6.96×10^{-3}	1.071
0.40	4.04×10^{-4}	1.180
0.50	1.15×10^{-3}	1.175

[a]The activation energy for ceria in Ref. 19.

for $Ce_{1-x}Nd_xO_{2-\delta}$ solid solutions increased from $\sigma = 1.12 \times 10^{-2}$ S cm^{-1} at $x = 0.10$ to $\sigma = 2.44 \times 10^{-2}$ S cm^{-1} at $x = 0.20$. When the dopant content was increased above $x = 0.20$, the ionic conductivity decreased continuously. By contrast, the activation energy showed a minimum of $E_a = 0.801$ eV at $x = 0.20$. Further increasing dopant content led to an increase of the activation energy. The activation energy of $E_a = 1.96$ eV for ceria[19] exactly follows such a trend. It is shown that $Ce_{1-x}Nd_xO_{2-\delta}$ solid solution was the most conductive phase among all compositions in $Ce_{1-x}Nd_xO_{2-\delta}$ with an ionic conductivity comparable to that of $\sigma = 2.8 \times 10^{-2}$ S cm^{-1} for $Ce_{0.8}Gd_{0.2}O_{2-\delta}$ at 700 °C,[20] the best conductive phase in $Ce_{1-x}Gd_xO_{2-\delta}$ solid solutions.[20,21]

For a good understanding of the mechanism for the variation trend in the conductivity data for $Ce_{1-x}Nd_xO_{2-\delta}$ solid solutions, the defect characteristics for the solid solutions should be considered. As revealed by XRD analyses, there exists some amount of oxygen vacancies $V_{\ddot{O}}$ and defect associations $\{Nd_{Ce}'V_{\ddot{O}}\}/\{Ce_{Ce}'V_{\ddot{O}}\}$ in the solid solutions. With increasing dopant content of Nd^{3+}, the content of oxygen vacancies $V_{\ddot{O}}$ increased, which accounted for the gradual increase in conductivity and decrease in the activation energy. At a dopant level higher than $x = 0.20$, the localized defect associations $\{Nd_{Ce}'V_{\ddot{O}}\}/\{Ce_{Ce}'V_{\ddot{O}}\}$ formed at the expense of the mobile oxygen vacancies, which accounted for the decrease of conductivity and increase of activation energy. The variation of the relative content of the oxygen vacancies and defect associations could be used to explain the conductivity maximum and activation energy minimum at $x = 0.20$. Similar results had been found in other doped ceria solid solutions.[22]

IV. CONCLUSIONS

This work reports on the solid solubility and transport properties of $Ce_{1-x}Nd_xO_{2-\delta}$ ($x = 0.05$ to 0.55) nanocrystalline solid solutions by a sol-gel route. It was found that cubic $Ce_{1-x}Nd_xO_{2-\delta}$ solid solutions had a solid solubility as high as about $x = 0.40$. The content of oxygen vacancies in the solid solutions increased with the dopant content, as was confirmed by Raman spectra. EPR spectra further revealed the presence of O_2^- on the sample surface and of Ce^{3+} with a low symmetry at lower dopant content. $Ce_{1-x}Nd_xO_{2-\delta}$ nanocrystalline solid solutions exhibited both relatively high thermal stability and enhanced ionic conductivity. Among all compositions, $Ce_{0.80}Nd_{0.20}O_{2-\delta}$ was determined to be a good conductive phase with a relatively high conductivity of $\sigma_{700\,°C} = 2.44 \times 10^{-2}$ S cm^{-1} and activation energy of $E_a = 0.802$ eV. The variations of the conductivity and activation energy could be closely related to the relative content of oxygen vacancies $V_{\ddot{O}}$ and defect associations $\{Nd_{Ce}'V_{\ddot{O}}\}/\{Ce_{Ce}'V_{\ddot{O}}\}$ in the solid solutions.

ACKNOWLEDGMENTS

This project was financially supported by a fund of the National Natural Science Foundation of China (NSFC) (No. 19804005) (L.L.). The authors thank the Japanese Ministry of Education, Science, Sports, and Culture for meeting the publication charge of this work.

REFERENCES

1. H. Inaba and H. Tagawa, Solid State Ionics **83,** 1 (1996).
2. S.C. Singhal, Solid State Ionics **135,** 305 (2000).
3. H.L. Tuller and A.S. Nowick, J. Electrochem. Soc. **122,** 255 (1975).
4. T.H. Etsell and S.N. Flengas, Chem. Rev. **70,** 339 (1970).
5. H. Yahiro, Y. Baba, K. Eguchi, and H. Arai, J. Electrochem. Soc. **135,** 2077 (1988).
6. I. Riess, Solid State Ionics **52,** 127 (1992).
7. G.B. Balazs and R.S. Glass, Solid State Ionics **76,** 155 (1995).
8. G. Li, Y. Mao, L. Li, S. Feng, M. Wang, and X. Yao, Chem. Mater. **11,** 1259 (1999).
9. L. Li, G. Li, Y. Che, and W. Su, Chem. Mater. **12,** 2567 (2000).
10. R.D. Shannon, Acta Crystallogr. A **32,** 751 (1976).
11. S.J. Hong and A.V. Virkar, J. Am. Ceram. Soc. **78,** 433 (1995).
12. W.H. Weber, K.C. Hass, and J.R. McBride, Phys. Rev. B **48,** 178 (1993).
13. J.R. McBride, K.C. Hass, B.D. Poindexter, and W.H. Weber, J. Appl. Phys. **76,** 2435 (1994).
14. V.G. Keramidas and W.B. White, J. Chem. Phys. **59,** 751 (1973).
15. C. Oliva, G. Termignone, F.P. Vatti, L. Forin, and A.V. Vishniakov, J. Mater. Sci. **31,** 6333 (1996).
16. M. Che, J.F.J. Kibblewhite, and A.J. Tench, J. Chem. Soc. Faraday Trans. **69,** 857 (1973).
17. R. EI-Mallawany, A.H. EI-Sayed, and M.M.H.A. EI-Gawad, Mater Chem. Phys. **41,** 87 (1995).
18. X. Lin, L. Li, G. Li, and W. Su, Mater. Chem. Phys. **69,** 236 (2001).
19. H.L. Tuller and A.S. Nowick, J. Electrochem. Soc. **126,** 209 (1979).
20. D.L. Maricle, T.E. Swarr, and S. Karavolis, Solid Ionic Ions **52,** 173 (1992).
21. N.Q. Minh, J. Am. Ceram. Soc. **76,** 563 (1993).
22. W. Huang, P. Shuk, and M. Greenblatt, Chem. Mater. **9,** 2240 (1997).